Geometrical Magnetothermopower in Semiconductors

Joseph P. Heremans, Christopher M. Thrush, and Donald T. Morelli
Delphi Research Labs, Delphi Automotive Systems, 51786 Shelby Parkway, Shelby Township, Michigan 48315
(Received 2 October 2000)

The geometry of a semiconductor sample can be designed to create a very large change of the thermoelectric power in a magnetic field, similar to the effects of the sample geometry on the magnetoresistance. In semiconductors in which the minority carriers have a higher mobility than the majority carriers, this geometrical magnetothermopower can freeze out the contribution of the former to the total thermopower. This opens a new route toward high-efficiency thermoelectric materials. We also examine the thermoelectric reciprocity relations for these macroscopic systems.

DOI: 10.1103/PhysRevLett.86.2098 PACS numbers: 72.20.Pa

Geometrical effects have been shown recently [1] to result in great enhancements of the magnetoresistance in narrow-gap semiconductors. It is the purpose of this Letter to show that similarly large effects can be obtained in the magnetic field dependence of the thermoelectric power, conceptually opening a new way to optimize the efficiency of materials used in thermoelectric converters.

It was observed 40 years ago [2] that the magnetothermopower of rectangular samples of $Bi_{93}Sb_7$ alloys depends on the length-to-width aspect ratio of the sample. However, geometrical magnetoresistance effects are known to be relatively small [3] compared to the intrinsic magnetoresistivity in multiband semiconductors with nonspherical carrier Fermi surfaces such as $Bi_{1-x}Sb_x$. Harman [4] reports the magnetothermopower in Corbino geometry (shown in Fig. 1) of n-type HgSe and derives the partial electron magneto-Seebeck coefficient; this was done on a semiconductor in which the majority carrier was the high-mobility carrier. Kaila and Goldsmid [5] report the thermomagnetic properties of InSb films that contained several phases of InSb and filamentary inclusions of metallic In. These films showed a geometrical magnetoresistance and magnetothermopower, to which the effect reported here may have contributed. It was shrouded, however, by the contributions of the many phases.

Geometrical effects can lead to a large magnetoresistance [3] in samples in which the Hall voltage is shorted out, such as samples shaped in the Corbino geometry. These effects are proportional to a power of the product of the carrier mobility and the magnetic field. In a rectangular geometry, the geometrical magnetoresistance is minimal [3] when the sample length (L) is much larger than its width (W), whereas it is maximal [3] when $L \ll W$. The limiting case where $L/W \rightarrow 0$ is equivalent to the Corbino geometry.

In this Letter, we show that, in a lightly doped semiconductor in which the minority carrier has the highest mobility, a geometry in which the Ettingshausen effect is shorted out can be used to freeze out the contribution of the minority carrier to the total thermopower. The result is a very large change of the thermopower with magnetic field, which we call a geometrical magnetothermopower (GMT).

The second question we address is the issue of the extension of the Onsager relations to macroscopic geometry-dependent transport. In microscopic linear transport, the electric and thermal current density vectors $\mathbf{J}$ and $\mathbf{U}$ are related to the electric and thermal field vectors $\mathbf{E}$ and $\nabla\mathbf{T}$ by a generalized Ohm's law, Eq. (12.4.2) in Ref. [6], in terms of a matrix of microscopic conductivities $\mathbf{L}$:

$$\begin{aligned} \mathbf{J} &= \mathbf{L}_{EE}(\mathbf{B}) \cdot \mathbf{E} + \mathbf{L}_{ET}(\mathbf{B}) \cdot \nabla\mathbf{T}, \\ \mathbf{U} &= \mathbf{L}_{TE}(\mathbf{B}) \cdot \mathbf{E} + \mathbf{L}_{TT}(\mathbf{B}) \cdot \nabla\mathbf{T}, \end{aligned} \tag{1}$$

where the resistivity tensor $\boldsymbol{\rho}$ is $\mathbf{L}_{EE}^{-1}$ and the thermopower tensor is $\mathbf{Q} = -\mathbf{L}_{EE}^{-1}\mathbf{L}_{ET}$, while the Peltier tensor is $\boldsymbol{\Pi} = +\mathbf{L}_{TE}\mathbf{L}_{EE}^{-1}$. The Onsager relations (12.4.5) [6] govern their reciprocity. One of the Onsager relations, $\boldsymbol{\Pi}(\mathbf{B}) = +T\mathbf{Q}^T(-\mathbf{B})$, mandates that the thermopower of a two-dimensional sample in the (x, y) plane is an even function of the field along the z direction, $Q_{xx}(B_z) = Q_{xx}(-B_z)$, and also gives the Kelvin relation: $\prod_{xx}(B_z) = +TQ_{xx}(-B_z)$. In a system with a defined geometry and contacts, the electrical and thermal currents in the contacts, I_i and U_i ($i = 1 \ldots n$, n being the number of contacts), are related to their voltages V_i and temperatures T_i (referred to an arbitrary zero, say $V_1 = 0, T_1 = 0$) by a generalized equation similar to Eq. (1) but describing the macroscopic conductances rather than the conductivities. For a two-contact system, such as shown in Fig. 1,

$$\begin{aligned} I_2 &= S(B)V_2 + L_{ET}(B)T_2, \\ U_2 &= L_{TE}(B)V_2 + L_{TT}(B)T_2, \end{aligned} \tag{2}$$

where $S(B) = 1/R(B)$ and R is the sample resistance, $K = -L_{TT} + RL_{TE}L_{ET}$ is the thermal conductance, the two-wire thermopower is $\alpha(B) = -RL_{ET}(B)$, and the Peltier coefficient is $\prod(B) = RL_{TE}(B)$. Butcher [7] studies the reciprocity of the conductance matrix elements for a system with two point contacts, and derives theoretically that the Kelvin relation $\prod = T\alpha$ holds, and that $\prod$ and α

 0031-9007/01/86(10)/2098(4)$15.00

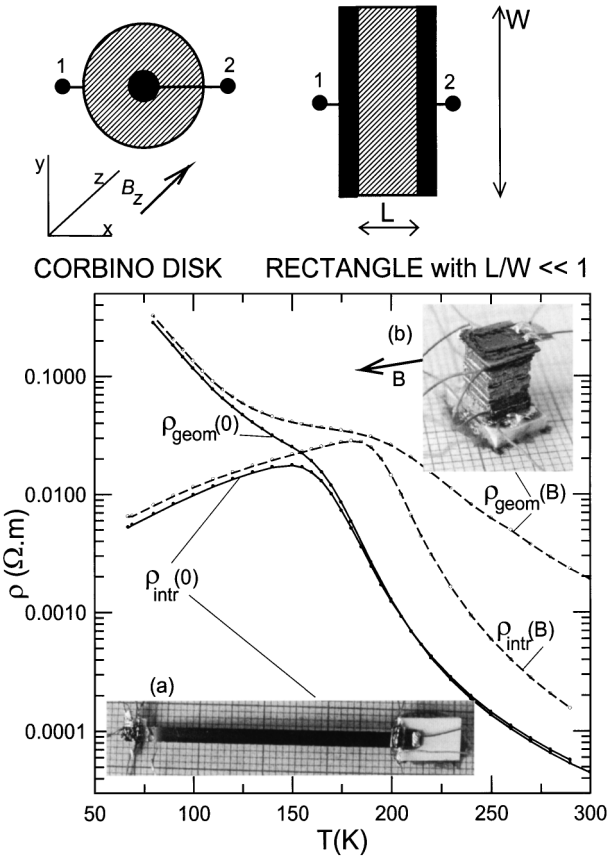

FIG. 1. Schematic representation of the Corbino disk geometry, compared to the rectangular geometry. The semiconductor area is hatched and the metal contacts are black. In a Corbino resistance measurement, current is applied between contacts 2 and 1, and the voltage is measured across them; in thermopower measurements, the heat flows from 2 to 1 and $\alpha = (V_2 - V_1)/(T_2 - T_1)$. The framed figure shows photos of the two samples (a) and (b), with L: $W = 18$ (a) and L: $W = 0.1$ (b). The magnetic field is applied normal to the plane of sample (a) and along the arrow for sample (b). The temperature dependence of the resistivity of both samples at zero field $[\rho(0)]$ and at $B = 1.85$ T $[\rho(B)]$ is shown. The magnitude of the intrinsic magnetoresistance is illustrated by the difference between $\rho_{\text{intr}}(0)$ and $\rho_{\text{intr}}(B)$. The geometrical magnetoresistance above 150 K is illustrated by the difference between $\rho_{\text{intr}}(B)$ and $\rho_{\text{geom}}(B)$. The increase of $\rho_{\text{geom}}(0)$ and $\rho_{\text{geom}}(B)$ with decreasing temperature below 150 K is a parasitic effect due to the contact resistance between the p-type material and indium metal.

are even functions of the magnetic field. Here, we verify this experimentally.

As far as practical applications are concerned, it is well known [8] that the intrinsic magnetothermopower of $Bi_{1-x}Sb_x$ alloys, which is due to their complicated band structure, greatly enhances their thermoelectric figure of merit in a magnetic field. The GMT described here can be used to achieve the same effect with any semiconductor, provided that the electrons and holes have different mobilities, and are scattered by acoustic phonons. One can view a thermomagnetic cooler based on a geometrical magneto-Peltier effect as related to a Nernst-Ettingshausen cooler, just as the Corbino magnetoresistance results from the suppression of the Hall voltage.

The material used in the experiment was bulk p-type Ge-doped InSb in the form of a 0.516 mm thick wafer. The carrier densities and mobilities of the material were first measured from 77 to 400 K. Below 140 K, the majority holes dominate the transport properties, with a density $p = 1.0 \times 10^{15}$ cm^{-3} and a mobility $\mu_h = 9\,300$ cm^2/V $\cdot$ s at 77 K. Above 190 K, the high-mobility minority electrons dominate the transport, their density being $n = 4 \times 10^{14}$ cm^{-3} and their mobility $\mu_e = 100\,000$ cm^2/V $\cdot$ s at 200 K. Two rectangular samples labeled (a) and (b), and shown in Fig. 1, were fabricated from the wafer. Sample (a) was cleaved from the wafer and lightly etched to minimize the surface recombination rate. It is $W = 2.2$ mm wide, and $t = 0.516$ mm thick. A heater and a current wire were attached on one end, and a heat sink (glued to the cold finger of the cryostat) and a second current wire were attached to the other. Voltage probes were In-soldered and a differential type-K thermocouple varnished on the sample, a length of $L = 40$ mm apart. Since $L/W \gg 1$, data taken on a sample (a) reflect the intrinsic properties of the material. Sample (b) consisted of a stack of seven 5×5 mm^2 pieces of the wafer, soldered together with indium. The indium shorts out the Ettingshausen and Hall voltages. Sample (b) was equipped with heater and heat sink, current wires, and voltage and temperature probes as sample (a). Sample (b) is equivalent to a set of seven samples with $L = 0.516$ mm, $W = 5$ mm, and $t = 5$ mm. Since $L/W \approx 0.1$, the geometrical magnetoresistance and magnetothermopower dominate its transport properties. Current/voltage characteristics were verified to be linear, except for sample (b) below 150 K, where a contact resistance appears, presumably at the In contacts to p-type InSb. Figure 1 illustrates the temperature dependence of the resistivity of both samples at zero field and at 1.85 T. The magnitude of the intrinsic and geometrical magnetoresistance is clearly illustrated.

Figure 2 shows the experimental temperature dependence of the thermopower of both samples, while Fig. 3 shows the magnetic field dependence of sample (b). The difference between the filled and the open triangles in Fig. 2(a) is the intrinsic magnetothermopower of the material, while the difference between the filled and open circles in Fig. 2(b) includes the GMT on top of the intrinsic one. It is clearly visible that, at all temperatures $T > 200$ K, the GMT effect is so large as to reverse the sign of the thermopower, a situation that the intrinsic magnetothermopower achieves only at $T < 200$ K. We see in Fig. 3 that the magnetic field dependence of the GMT above 190 K is not saturated at the 1.85 T field available to us; the data were extrapolated to infinite field, following the procedure described by Aliev *et al.* [9]. The temperature dependence of this extrapolation is shown as a dash-dotted line in Fig. 2(b). The thermopower of the InSb/In composite sample (b) is defined as the ratio of the voltage

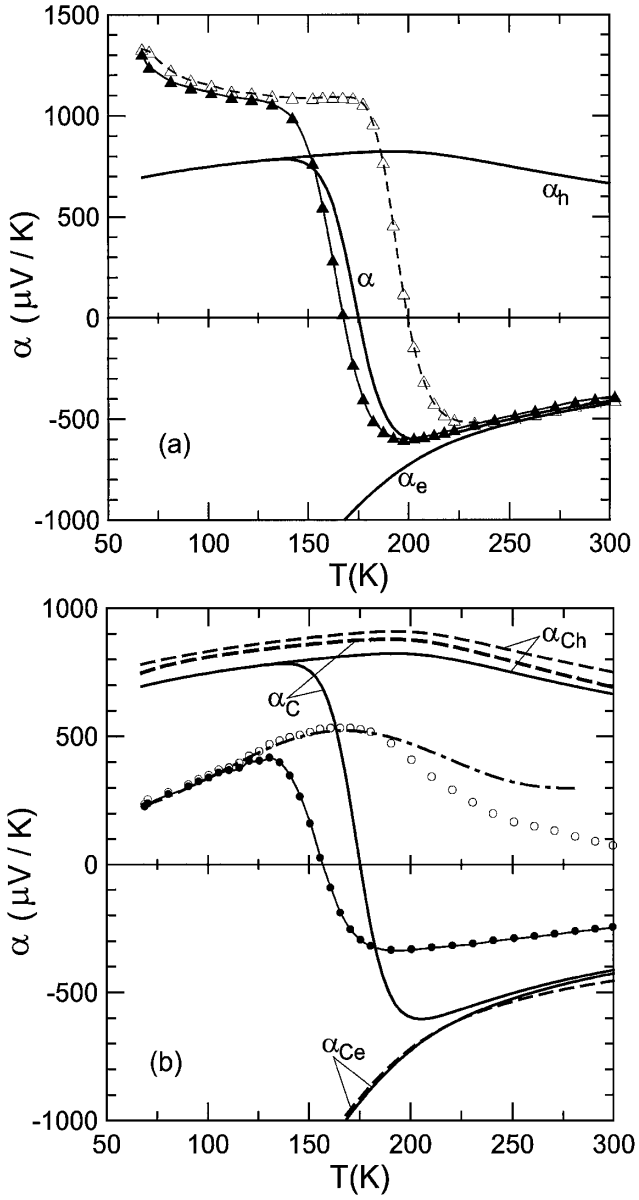

FIG. 2. Temperature dependence of the experimental thermopower of sample (a), top frame, and sample (b), bottom frame, at zero magnetic field (closed data points) and at 1.85 T (open data points). The thick full lines are the calculated partial (α_e and α_h) and total (α) thermopowers at zero magnetic field, the thick dashed lines the same at the limit of $\mu B \gg 1$. The dash-dotted line in the bottom frame shows the thermopower of sample (b) extrapolated to $\mu B \gg 1$.

drop to the total temperature gradient between the probes. Sample (a) had a thermal conductivity κ_a equal to a multiple β of the thermal conductivity, κ_b, of the composite sample (b). When plotted as a function of temperature, $\beta = \kappa_a/\kappa_b$ varies between 1.7 (at 200 K) and 2.3 (at 100 and 300 K), so that we assume that $\beta \approx 2$. The temperature gradient across the composite is thus distributed half across the InSb, and half across the In/InSb contacts. The corrected thermopower due to the InSb with short L/W ratio is thus about double the value shown in Figs. 2(b) and 3. The increase in thermopower below 100 K observed in Fig. 2(a) is due to phonon drag [10], a phenomenon not included in the following model.

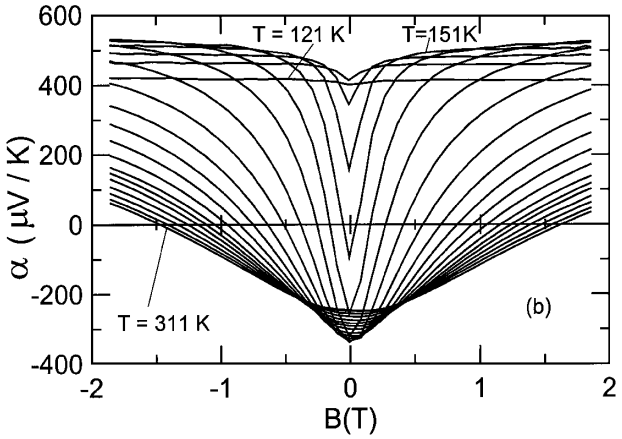

FIG. 3. Magnetic field dependence of the thermopower of sample (b). The temperatures decrease by 10 K from the bottom curve (labeled 311 K) to the top one (151 K), then decrease again in 10 K steps to 121 K.

The explanation for the GMT effect is as follows. At zero magnetic field, the thermopower is dominated by the majority holes at $T < 140$ K, but by the minority electrons at $T > 180$ K, because the electron mobility is much higher than the hole mobility. The magnetic field B impedes carrier transport, leading to magnetoresistance, but electrons are more affected than holes because they have a higher mobility μ, and the magnetoresistance effects are proportional to a power of μB. The intrinsic magnetoresistance thus leads to a sign reversal of the thermopower at $140\ \text{K} < T < 200$ K, while the geometrical magnetoresistance does so even at room temperature, because it is a much larger effect, as seen in Fig. 1.

Quantitatively, for the microscopic case represented by sample (a), the thermoelectric power α of a semiconductor is given by the average of the partial thermopowers (α_e and α_h) of electrons and holes, weighted by their respective partial electrical conductivities [11]:

$$\alpha = \frac{\alpha_e \sigma_e + \alpha_h \sigma_h}{\sigma_e + \sigma_h}. \tag{3}$$

The partial electrical conductivities in the absence of a magnetic field are $\sigma_e = ne\mu_e$ and $\sigma_h = pe\mu_h$, where n and p are the electron and hole densities, μ_e and μ_h their mobilities, and e is the electron charge. The partial thermopowers, in the absence of a magnetic field, are known [11] to be functions of the partial Fermi energies of the carriers, the energy gap for the nonparabolic band, and the scattering exponent λ defining the energy dependence of the scattering time $\tau = \tau_0 E^\lambda$. For polar optical phonon scattering, $\lambda = \frac{1}{2}$; for ionized impurity scattering, $\lambda = \frac{3}{2}$; and $\lambda = -\frac{1}{2}$ for acoustic phonon scattering. The magnetic field affects the partial thermopowers, which are described by Harman [11] for the limit $\mu B \gg 1$. The partial conductivities are also affected, but Eq. (3) holds.

We model sample (b) as a Corbino disk, assuming the Hall and Ettingshausen voltages shorted out. Harman [11] summarizes the equations for the partial thermopowers, defined as α_{Ce} and α_{Ch} in this geometry. At zero field, they are the same as for the case $L \gg W$, but not at high field ($\mu B \gg 1$). However, the differences between the partial thermopowers at $B = 0$ and at $\mu B \gg 1$, for either $L/W \ll 1$ or $L/W \gg 1$, are much smaller than the GMT effect described here. In our model, the total thermopower α_C is now given by the average of the partial thermopowers weighed by the partial conductances, G_e and G_h, of electrons and holes in the particular geometry studied:

$$\alpha_C(B) = \frac{\alpha_{Ce} G_e(B) + \alpha_{Ch} G_h(B)}{G_e(B) + G_h(B)} . \qquad (4)$$

For $L/W = 0$, Ref. [3],

$$G_e \propto \frac{ne\mu_e}{1 + \mu_e^2 B^2}, \qquad G_h \propto \frac{pe\mu_h}{1 + \mu_h^2 B^2} , \qquad (5)$$

so that, for $\mu_e > \mu_h$,

$$\lim_{B\to 0}[\alpha_C(B)] = \alpha_{Ch} . \qquad (6)$$

As the carrier densities and mobilities are known from the Hall measurements, the partial Fermi energies can be calculated, and also the partial and total thermopowers. In our model for InSb, both conduction and valence bands are assumed isotropic, with the conduction band dispersion relation nonparabolic. There are no adjustable parameters. The calculations are not very sensitive to the assumptions made about the scattering mechanism; we assumed acoustic phonon scattering. The details will be given elsewhere [12]. The results are shown in Fig. 2. Clearly, the experimental data are well reproduced, and the features of the dashed line α_C follow the experimental dash-dotted line quite well, given the factor of $\beta \approx 2$.

We now consider the macroscopic equivalent of the Kelvin relation. The experimental Peltier coefficient of sample (b) is compared in Fig. 4 to the experimental values of $\beta T \alpha(B)$ on the same sample, where the factor $\beta \approx 2$ takes into account the temperature gradient across the In/InSb contacts. The agreement is consistent with the existence of a Kelvin relation for two-wire macroscopic samples. Note that $\alpha(B) = \alpha(-B)$ in Fig. 3, but this is also a consequence of the geometrical symmetry of sample (b) with respect to B.

Can we use the GMT to increase the thermoelectric figure of merit Z? Calculations [12] of the power factor [11] $\alpha^2\sigma$ as a function of doping level in the presence of the GMT show that this quantity may be increased by as much as 80%, if we assume scattering of carriers by acoustic phonons. As the thermal conductivity is dominated by lattice conduction, this improvement also holds for Z.

In summary, the GMT effect described here in samples with a geometry in which the Hall and Ettingshausen voltages are shorted can create a very large magnetic field dependence of the thermoelectric power of semiconductors in which the minority carriers have a higher mobility than the majority carriers. A macroscopic relation exists in this geometry between the Peltier coefficient and the Seebeck coefficient, similar to the microscopic Kelvin relation. By analogy with the effect of the intrinsic magnetothermopower on the figure of merit of $Bi_{1-x}Sb_x$ alloys, the GMT effect can generate an enhancement of the thermoelectric figure of merit of semiconductors with spherical Fermi surfaces by as much as a factor of 1.8, when acoustic phonon scattering dominates.

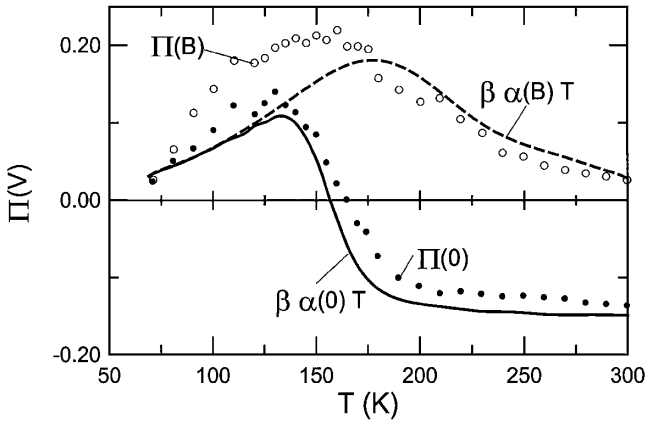

FIG. 4. Peltier coefficient of sample (b) as a function of temperature. The closed dots are the experimental data points at $B = 0$, the open dots at $B = 1.85$ T. The lines, full at $B = 0$, dashed at $B = 1.85$ T, give the experimental values of $\beta T \alpha$, with $\beta = 2$.

We acknowledge Professor H. J. Goldsmid and Dr. D. R. Baker for very useful discussions.

[1] S. A. Solin, T. Thio, D. R. Hines, and J. J. Heremans, Science **289**, 1530 (2000).
[2] M. E. Ertl, G. R. Pfister, and H. J. Goldsmid, Br. J. Appl. Phys. **14**, 161 (1960).
[3] D. R. Baker and J. Heremans, Phys. Rev. B **59**, 13 927 (1999).
[4] T. C. Harman, Phys. Rev. **118**, 1541 (1960).
[5] M. M. Kaila and H. J. Goldsmid, Phys. Status Solidi (a) **28**, K167 (1975).
[6] J. M. Ziman, *Electrons and Phonons* (Oxford University, New York, 1979).
[7] P. N. Butcher, J. Phys. Condens. Matter **2**, 4869 (1990).
[8] W. M. Yim and A. Amith, Solid State Electron. **15**, 1141 (1972).
[9] S. A. Aliev, L. L. Korenblit, and S. S. Shalyt, Sov. Phys. Solid State **8**, 565 (1966).
[10] A. P. R. Frederikse and E. V. Mielczarek, Phys. Rev. **99**, 1889 (1955).
[11] T. C. Harman and J. M. Honig, *Thermoelectric and Thermomagnetic Effects and Applications* (McGraw-Hill, New York, 1967).
[12] J. Heremans, C. M. Thrush, and D. T. Morelli, in Proceedings of the 19th International Conference on Thermoelectricity, Cardiff, United Kingdom, 2000 (to be published).